Applied Physics Letters

Wave-driven non-classical electron transport in a low temperature magnetically expanding plasma

Cite as: Appl. Phys. Lett. **116**, 263502 (2020); https://doi.org/10.1063/5.0012668
Submitted: 03 May 2020 . Accepted: 09 June 2020 . Published Online: 01 July 2020

Shadrach Hepner, Benjamin Wachs, and Benjamin Jorns

ARTICLES YOU MAY BE INTERESTED IN

Applied Physics Letters ARTICLE scitation.org/journal/apl

Wave-driven non-classical electron transport in a low temperature magnetically expanding plasma

Cite as: Appl. Phys. Lett. **116**, 263502 (2020); doi: 10.1063/5.0012668
Submitted: 3 May 2020 · Accepted: 9 June 2020 ·
Published Online: 1 July 2020

Shadrach Hepner,[a)] Benjamin Wachs,[b)] and Benjamin Jorns[c)]

AFFILIATIONS

Department of Aerospace Engineering, University of Michigan, Ann Arbor, Michigan 48109, USA

[a)]Author to whom correspondence should be addressed: shadrach@umich.edu
[b)]Electronic mail: bwachs@umich.edu
[c)]Electronic mail: bjorns@umich.edu

ABSTRACT

The presence of instabilities in a low density, low temperature plasma expanding through an axially symmetric magnetic nozzle is investigated in the context of non-classical electron cross field transport. Electrostatic probes are used to characterize the background plasma properties and instabilities. The measurements show a primarily azimuthally propagating mode with a broad, incoherent power spectrum that appears linear at low frequencies. It is demonstrated that the observed dispersion is consistent with the lower hybrid drift instability. The energy and linear growth rate of this wave are related through quasilinear theory to an effective electron collision frequency that is shown to be dominant over classical collisions.

The non-classical transport of charged particles across an expanding magnetic field plays an important role in a number of plasma physics subfields ranging from large-scale fusion[1,2] and astrophysical systems[3,4] to compact, low temperature plasmas.[5–8] This phenomenon is especially relevant for the magnetic nozzle (MN), an electric propulsion concept that leverages the expanding field geometry to convert thermal energy into directed flow.[9–13] In MNs, cross field transport is critically linked to the process of detachment, whereby the expanded plasma ultimately decouples from the magnetic field. Without a mechanism to detach, plasma will return along the field lines, negating thrust. To date, although there have been a number of proposed theoretical mechanisms for electron detachment in MNs including classical electron resistivity,[14] finite electron inertia,[8,15,16] and magnetic field line stretching,[17,18] there is yet to be a consensus about which, if any, is dominant.[9,19] The lack of a clear mechanism to explain the electron transport suggests that there may be other as of yet undiscovered processes in the plasma. Given that the plumes of these low temperature devices are typically characterized by strong cross field gradients in potential and density, there is reason to believe—as has been seen in similar systems[7,20]—that drift waves may play a governing role in enhancing particle transport. However, there has been no direct experimental evidence of cross field, drift instabilities in this plasma configuration, or link to the transport they may induce. In light of this, the goal of this investigation is to explore experimentally the transport-inducing instabilities in the plume of a low temperature MN and to relate their presence to an effective transport term. To this end, we describe, in this Letter, the use of a two-point probe technique to measure the wave properties in a canonical low temperature MN geometry; we interpret the measured dispersion in the context of the linear theory of the lower hybrid drift instability (LHDI); and we employ quasilinear theory to relate the energy in the measured waves to an enhanced, non-classical electron transport term.

Figure 1 shows the microwave-driven MN we used for this study as well as the magnetic field topology and coordinate conventions. This MN is based on the design of Cannat *et al.*[21] and Wachs and Jorns[22] where a diverging magnetic nozzle is formed by annular permanent magnets, and electron cyclotron resonant heating is employed to generate the plasma via a coaxial antenna. During testing, the device was operated at 17 W with 2 sccm of xenon fed radially into the upstream portion of the 25 mm diameter discharge region. We conducted tests in the Junior vacuum facility at the University of Michigan, a cylindrical chamber 1 m in diameter and 3 m in length with an operating backpressure of 4.3×10^{-6} Torr measured at the wall.

We employed two sets of translating probes to measure the time-varying and steady-state plume properties in the MN as shown in Fig. 1(b). For time-varying measurements, we adopted a two-point measurement technique where we used orthogonal pairs of cylindrical

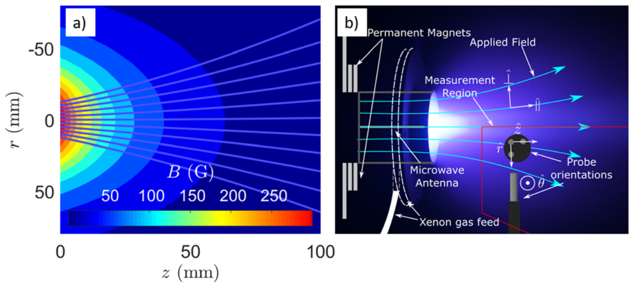

FIG. 1. (a) Magnetic field contours, $\vec{B}$, and strength B of the MN and (b) Image of the MN operating on xenon along with notional probe orientations (not to scale) and coordinate conventions. The probes were operated in two orientations. In the first, their axis of symmetry was in the $\hat{\theta}$ direction (out of the page). In the second, it was in the -$\hat{r}$ direction (toward the centerline). The thruster has a diameter of 25 mm at the exit plane ($z = 0$).

probes 5 mm in length and 1 mm in diameter biased to ion saturation. These pairs were separated by 7 mm in the $\hat{r}$ and $\hat{z}$ directions and 5 mm in the $\hat{\theta}$ direction. Following the histogram-based approach of Refs. 23–26, we used the temporal and spatial correlations of the relative fluctuations of ion saturation current $\tilde{i}_{sat}/\bar{i}_{sat}$ to estimate the wave dispersion and power spectra. For steady-state plasma properties, we employed a swept Langmuir probe of the same dimensions to characterize the plasma density, plasma potential, and electron temperature. Given the known non-thermal nature of the electrons in ECR sources, we followed the approach of Ref. 27 in using the moments of the electron energy distribution to determine the temperature, followed the industry-standard orbital motion limited procedure[28] for the density, and found potential using the standard first-derivative technique.[28] We moved both the Langmuir and wave probe sets through the $\hat{r} - \hat{z}$ plane of the thruster, yielding spatially resolved measurements of the plasma properties over a domain 30–150 mm downstream from the thruster exit and 0–130 mm radially from the centerline.

Figure 2 shows the measured plasma potential and plasma density in the MN plume. We do not show the electron temperature T_e as we found it to be approximately isothermal throughout the measurement domain $\approx 13 \pm 2$ eV. As shown in Fig. 2, the monotonic

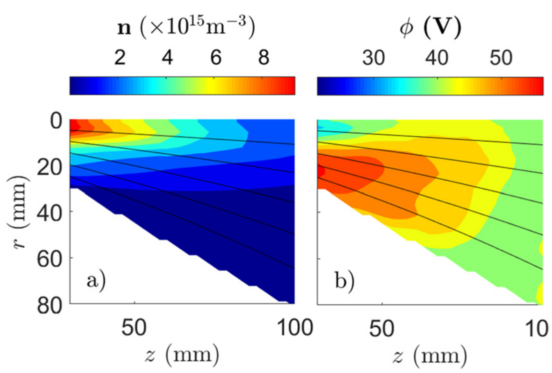

FIG. 2. Two-dimensional maps of (a) plasma density n and (b) plasma potential ϕ at an operating condition of 17 W power and 2 sccm xenon flow rate. The black lines represent magnetic field lines. The axial origin ($z = 0$) is defined to be at the exit of the discharge chamber.

decrease in density downstream of the source is an indication of the expansion of the plume. The potential profiles follow a similar trend, decreasing monotonically in magnitude from the source. This potential profile is the consequence of an ambipolar field established between ions and electrons and is responsible for ion acceleration. Similar plasma property distributions have been observed in previous work[27,29] although in a significant departure from the most recent study by Little and Choueiri,[8] we do not observe potential wells (characterized by an off-axis increase in the potential) at the vacuum-plasma interface (defined by the outermost magnetic field line that intersects the exit plane). The potential instead decreases smoothly and monotonically in the radial direction outside of $r \approx 20$ mm, with the exception of a small dip that appears closest to the MN exit plane. The latter feature may be a consequence of the presence of the central conducting pin obstructing the plasma although we note that similar potential wells have been noted in ECR plasma sources in previous work.[30] According to this reference text, the formation of the potential peak-off center may be a response to upstream ions diffusing faster than the more magnetized electrons due to a finite ion temperature. For the purpose of this study, however, the most salient feature is the existence of strong density and potential gradients off the centerline and across the confining magnetic field topology. These gradients drive the azimuthal drifts that can serve as the energy source for the onset of instabilities.

With this in mind, we show in Fig. 3 examples of dispersion measurements in three directions $(\hat{r}, \hat{z}, \hat{\theta})$ at $(r, z) = (25, 50)$ mm. These results show the intensity of relative ion saturation fluctuations as a function of wavenumber normalized by the electron Larmor radius, $r_L = \frac{m_e v_{te}}{eB}$ (3 mm locally), and frequency normalized by the ion plasma

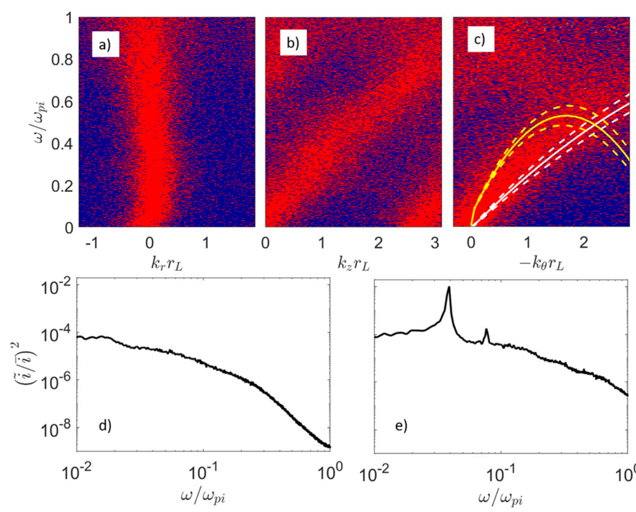

FIG. 3. Measured dispersion relation in the (a) radial, (b) axial, and (c) azimuthal directions at the location z = 50 mm and r = 25 mm where the plot color scale has been saturated to illustrate the trends. (d) The power spectral density at the same point as (a)–(c); (e) the power spectral density at z = 110 m and r = 50 mm. The white and yellow lines in (c) are the theoretical real solution and 10× the growth rate, respectively, of Eq. (1), with confidence bars represented by dashed lines. Each plot presents frequencies and wavenumbers normalized to the plasma frequency and Larmor radius, respectively (left, bottom axes) as well as physical values (right, top axes).

frequency (4.4 MHz). Here, we have corrected for an aliasing in the wavenumber that stems from the finite distance between probe tips by following the procedure in Ref. 31 and concatenating the measured datasets. This correction is the reason for the duplicate structures, such as the traces in the upper left and lower right of Fig. 3(b). The dispersion plots show that while there is little dispersion in the radial direction, there is an evident relationship between frequency and the wave number in both the azimuthal and axial directions. This suggests the waves are propagating in both directions with frequencies extending up to the local ion plasma frequency. These characteristics are consistent with the physical interpretation that instabilities can be driven unstable by gradient-driven electron drift in these devices.

Figure 3(d) shows the power spectral density corresponding to the dispersion plots in Figs. 3(a)–3(c). These results indicate that these oscillations are broadband and turbulent in nature characterized by an inverse power law decay with frequency. We note that although we found that these azimuthal broadband modes persisted throughout the measurement domain, at the downstream edge ($z > 70$mm), we also observed a more coherent oscillation superimposed on the power spectrum at approximately 13 kHz and a harmonic at 26 kHz [c.f. Fig. 3(e)]. There were no unambiguous trends in dispersion for these modes although similar low-frequency oscillations have been observed before in MNs and attributed to longitudinal ion acoustic or ionization waves.[32,33] As the low frequency modes we measured did not appear everywhere and were not unambiguously azimuthal, we focus instead on a more detailed analysis of the broadband oscillations in the drift direction.

To this end, we can interpret the dispersion measurements in the context of the linear theory for drift-driven waves in low temperature plasmas. There are several salient features of the dispersion that guide us. First, we consider the potential energy sources for wave growth. There are two possible electron drifts in the plasma that may contribute to growth, the diamagnetic, $\vec{v}_D = (T_e \nabla n \times \vec{B})/(en|\vec{B}|^2)$, and $\vec{E} \times \vec{B}$ drift, $\vec{v}_E = (\vec{E} \times \vec{B})/(|\vec{B}|^2)$, where $\vec{E} = -\nabla\phi$ is the electric field. Using these expressions and the results in Fig. 2, we have found that the diamagnetic drift is on average an order of magnitude higher than the $\vec{E} \times \vec{B}$ drift. Furthermore, it is universally in the same direction as the wave propagation. The $E \times B$ drift, however, switches sign at approximately $r = 20$ mm, as evidenced by the potential peak implying a reversal of the electric field direction. This suggests at least by correlation that the diamagnetic drift is the dominant energy source. Second, Fig. 3(a)–3(c) show that the perpendicular wavelength is comparable to the electron Larmor radius. This implies that the wave is characterized by finite Larmor radius (FLR) effects and is, therefore, likely kinetic in nature. Finally, we measure finite propagation parallel to the magnetic field.

Taken together, these features of the dispersion suggest that the observed mode may be a lower hybrid drift instability (LHDI) with finite parallel propagation.[34,35] Indeed, the LHDI with parallel propagation is driven unstable by an electron pressure gradient; it propagates in the direction of the electron diamagnetic drift velocity[34,36]; it is characterized by FLR effects; and in low temperature, partially magnetized plasmas, it has been observed to exhibit a broadband power spectrum.[36] Moreover, the LHDI previously has been proposed as a dominant instability in higher power, fully magnetized nozzles[37,38] and appears prominently in magnetic reconnection transport studies.[35,36,39–43]

To analyze the LHDI in our MN, we consider a dispersion relation adapted from the form derived by Carter *et al.*[36] in which they assumed a Maxwellian distribution of electron speeds in Cartesian coordinates, allowed for finite propagation parallel to the magnetic field and FLR,

$$0 = 1 - \frac{\omega_{pi}^2}{(\omega + k_\perp v_E)^2} + \frac{1}{k^2\lambda_D^2} \times \left[1 + \frac{\omega - k_\perp v_D}{k_{||} v_{te}} e^{-k_\perp^2 r_L^2/2} I_0\left(\frac{k_\perp^2 r_L^2}{2}\right) Z\left(\frac{\omega}{k_{||} v_{te}}\right)\right], \quad (1)$$

where v_{te} is the electron thermal velocity, I indicates a modified Bessel function of the first kind, and Z is the plasma dispersion function. In departure from Ref. 36, which derived their result in the frame of reference of zero electric field, we instead show the form in the ion frame of reference. We have also made the assumption that ions are much colder than electrons, $T_i \ll T_e$, and that the phase velocity component in the parallel direction is larger than the parallel electron drift, $\omega/k_{||} \gg v_{e||}$. The latter criterion is valid, provided that the electron drift speed is ambipolar (i.e., comparable to the ion drift speed).[15,44]

In order to compare the theoretical result with our measurements, we use the probe results to estimate the terms in Eq. (1). The electron drift speeds are informed by the gradients in Fig. 2, and we determine the local experimental values of $k_{||}$ by projecting the propagation vector (k_r, k_z) onto the local magnetic field. With these estimates, we then solve Eq. (1) numerically for both real and imaginary components of the frequency as a function of perpendicular wavenumber, $\omega(k_\perp)$. Figure 3 shows the result along with estimated confidence intervals. We generated these trends by assuming that the uncertainty in the plasma measurements (according to Ref. 28) is normally distributed, randomly sampling from these distributions, and recalculating the dispersion. The indicated results reveal that the real component of the solution matches the measured dispersion within uncertainty. It is particularly notable that the change in the slope with the wavenumber is also reflected by the theoretical result. Moreover, the imaginary component of the frequency is positive for all wavenumbers, indicating that LHDI waves are unstable and can spontaneously onset for these plasma conditions. Coupled with the marked agreement with the real dispersion, this fact suggests that the wave is likely LHDI.

Indeed, while we only show the comparison for one location in the plume, we found that the LHDI was unstable at all locations in the plasma and that the real component of the predicted relation matched the shape and direction of the measured dispersion everywhere. With that said, there were some regions where the magnitude of the predicted frequency differed by up to a factor of four from measurements. These areas were concentrated off center and upstream ($r \gtrsim 20$ mm, $z \lesssim 70$ mm). This is not unexpected; however, given the number of simplifying assumptions, we employed Eq. (1). For example, these periphery regions near the vacuum interface have been shown to be characterized by effects not included in this derivation such as departures from quasineutrality.[8] The fact that we see marked agreement over the majority of plumes is quite notable considering the simplifications made in deriving Eq. (1).

Given the evidence that the observed modes are LHDI, we finally can turn to the central question regarding its role in electron transport in the MN plume. Indeed, the growth of the LHDI has already been linked to enhanced cross field motion in a number of other plasma configurations.[36,45,46] To evaluate its potential impact for our system, we adopt a quasilinear approach in which we introduce a transport coefficient, an effective collision frequency, attributed to the LHDI. Physically, this coefficient represents the rate at which the wave grows at the expense of the electron momentum. As the electrons lose energy to the wave growth, they slow down in a manner that manifests as a resistive drag force. This drag coupled with the background magnetic field facilitates a cross field ($\hat{\perp}$) motion of the electrons. Following Refs. 36 and 47, the quasilinear form for the effective collision frequency from the LHDI can be expressed as $\nu_{eff} = \frac{q}{n_e m_e v_{e_\theta}} \langle \delta E_\theta \delta n \rangle$, where δ indicates an oscillating property and angle brackets imply a phase average. We use the theoretical expressions for these perturbed quantities from Ref. 36 to write

$$\nu_{eff} = \frac{v_{te}^2}{2 v_D} \mathrm{Im}\left\{ \sum_{\omega} \left(\frac{\delta n_\omega}{n}\right)^2 k \left[1 + (\omega - k_\perp v_D) \times \frac{1}{k_\parallel v_{th,e}} Z\left(\frac{\omega}{k_\parallel v_{t,e}}\right) e^{-(k r_L)^2/2} \mathrm{I}_0\left((k r_L)^2/2\right)\right]^{-1} \right\}, \tag{2}$$

where $k = \sqrt{k_\perp^2 + k_\parallel^2}$ is the total wavenumber, δn_ω denotes the density fluctuation for the component of the LHDI spectrum oscillating at frequency ω, and the summation is over all frequencies in the spectrum. To evaluate Eq. (2), we use the measured values of the plasma properties inferred from Fig. 2 and the linear dispersion to relate ω and $k_\perp$. For the density fluctuations at each frequency, we make the approximation that the measured ion saturation current scales with the density fluctuations, $\tilde{i}_{sat}/\bar{i}_{sat} = \tilde{n}/n$.[31,48] Following this approach, we show the inverse calculated collision frequency in Fig. 4, where we have normalized at each location by the local cyclotron frequency. This plot, thus, shows the electron Hall parameter, $\Omega_e = \frac{eB}{m_e \nu}$, which is a relative measure of the magnetization of the electrons. For comparison, we also show the Hall parameter due to the classical electron-ion collision frequency (Ref. 49), defined in this situation to be $2.18 \times 10^{-11} n T_e^{-3/2}$ for singly charged xenon ions.

The resulting spatial plots illustrate that the Hall parameter attributed to the LHDI is several orders of magnitude lower than its classical equivalent, indicating that it has a non-negligible impact on electron transport. Indeed, in the downstream region ($z > 100$ mm), the Hall parameter drops below 100, whereas classically, the Hall parameter is over 10 000. While this decrease in the Hall parameter is

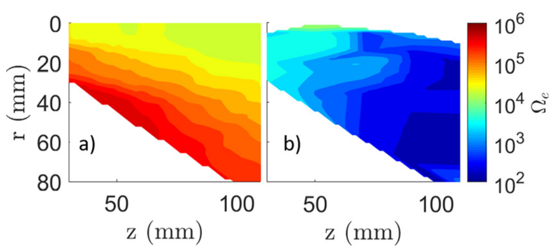

FIG. 4. Spatial dependence of the Hall parameter for assuming (a) classical and (b) wave-driven collision frequencies. The axial origin ($z = 0$) is defined to be at the exit of the discharge chamber.

substantial, values of 100 may still seem to imply confinement. However, we note that similar values have been determined to be sufficient to alter electron streamlines substantially in other crossed-field low temperature plasmas.[50] Moreover, if we assume an electron velocity in the $r - z$ plane that is comparable to the ion velocity[51] (around 10 km/s, estimated from a previous experiment on this thruster[52]), we can calculate a mean free path corresponding to the effective collision frequency. This value is around a centimeter, which is less than the thruster diameter and much less than the transit length through the plume, implying that electrons are affected by these effective collisions. Furthermore, relating these results back to previous MNs, we remark that Little and Choueiri concluded that the effective electron collision rate would need to be two orders of magnitude higher than the classical value to yield transport effects comparable to the FLR effect they studied.[8] Our results show that, at least for our MN, the role of instabilities may account for this two order of magnitude shortfall (Fig. 4). In light of these previous observations, our results in Fig. 4 suggest that the role of wave-driven resistive effects in electron detachment cannot be ignored.[8,9]

With this in mind, this non-classical resistivity will have a direct impact on the electron trajectories and thruster performance. As the LHDI grows at the expense of the diamagnetic drift, the effective azimuthal drag on the electrons combined with the magnetic field will push the electron trajectories radially outward and down the pressure gradient. This notably is in the same direction as predicted from FLR detachment.[8,53] As discussed in these previous works, the increased divergence of the electrons drives a radially directed ambipolar field that pulls the ions away from the thruster centerline. Even the ions close to the centerline that are confined by the off-axis potential peak [Fig. 2(b)] are likely affected, as increased radial transport of electrons would lower this barrier, allowing ions to expand as well. Although the effect is likely smaller for this population, the net effect qualitatively is an increased divergence and lower thrust. However, we cannot quantify the degree to which this effect will adversely impact thrust as we do not have a direct measurement of the ion and electron trajectories. We also note that while the LHDI will drive divergent electron detachment, it cannot be the only detachment mechanism for the electrons. Indeed, for the MN ultimately to produce thrust, the electrons must detach inward to follow the more convergent ions and maintain quasineutrality. This is in the opposite direction of motion that we anticipate based on the non-classical, wave-driven effect. Thus, while we anticipate based on our results that non-classical effects cannot be ignored in addressing the electron dynamics of our MN, the problem of global detachment and subsequent recombination of the species downstream remains an open question.

In summary, we have observed in this study azimuthally propagating waves in a low temperature, partially magnetized MN subject to an expanding magnetic field. We have determined based on linear dispersion relations that the observed instability is likely an LHDI, and we have discussed the implications of this mode on the macroscopic transport properties of the nozzle. While we have only considered the LHDI dispersion relation under the simplifying assumption of a uniform magnetic field, we show here that this linear relation still appears to be valid–agreeing quantitatively with wave measurements—in our expanding geometry. We have further explored the effect that the LHDI has on electron transport and concluded that it can enhance the effect of resistive transport by two orders of magnitude and, in turn, may lead to divergence. The discovery of non-classical transport in this class of low temperature plasmas has broad implications in the field. Indeed, while turbulence-driven cross field transport is a well-established phenomenon in large scale, higher energy plasmas such as those encountered in energy research[54] and astrophysical systems, we have shown here that this effect is dominant in a lower temperature device. This suggests that classical theory for transport may need to be revisited in a wider range of low temperature plasma systems such as in probe analysis techniques[55,56] and confined plasmas employed for plasma material interactions.[57] For MNs in particular, our finding that non-classical transport may dominate the electron dynamics is a paradigm shifting result for the understanding of electron detachment where historically such resistive effects have been neglected.

This work was funded under NASA Space Technology and Research Fellowship Grant No. 80NSSC17K0156.

DATA AVAILABILITY

The data that support the findings of this study are available from the corresponding author upon reasonable request.

REFERENCES

1. E. Austin, M.,A. Marinoni, M. L. Walker, M. W. Brookman, J. S. DeGrassie, A. W. Hyatt, G. R. McKee, C. C. Petty, T. L. Rhodes, S. P. Smith, C. Sung, K. E. Thome, and A. D. Turnbull, Phys. Rev. Lett. **122**, 115001 (2019).
2. V. P. Budaev, L. M. Bogomolov, B. V. Borovsky, R. S. Ivanov, E. D. Lazarev, A. V. Nedospasov, A. A. Rakovets, V. N. Sychev, Y. A. Trapeznikov, and A. V. Chernylevsky, J. Nucl. Mater. **176**, 705–710 (1990).
3. M. Faganello, F. Califano, and F. Pegoraro, Phys. Rev. Lett. **100**, 015001 (2008).
4. F. Califano, M. Faganello, F. Pegoraro, and F. Valentini, Nonlinear Process. Geophys. **16**, 1–10 (2009).
5. J. Jara-Almonte, H. Ji, J. Yoo, M. Yamada, W. Fox, and W. Daughton, Phys. Rev. Lett. **122**, 015101 (2019).
6. E. E. Lawrence, H. Ji, M. Yamada, and J. Yoo, Phys. Rev. Lett. **110**, 015001 (2013).
7. S. Tsikata and T. Minea, Phys. Rev. Lett. **114**, 185001 (2015).
8. J. M. Little and E. Y. Choueiri, Phys. Rev. Lett. **123**, 145001 (2019).
9. E. Ahedo and M. Merino, Phys. Plasmas **17**, 073501 (2010).
10. K. Takahashi, H. Akahoshi, C. Charles, R. W. Boswell, and A. Ando, Phys. Plasmas **24**, 084503 (2017).
11. K. Takahashi, T. Lafleur, C. Charles, P. Alexander, and R. W. Boswell, Phys. Rev. Lett. **107**, 235001 (2011).
12. C. Charles, J. Phys. D: Appl. Phys. **42**, 163001 (2009).
13. K. Takahashi, Rev. Mod. Plasma Phys. **3**, 3 (2019).
14. R. W. Moses, R. A. Gerwin, and K. F. Schoenberg, in Proceedings of the 9th Symposium Space Nuclear Power Systems (1992), Vol. 246, pp. 1293–1303.
15. E. B. Hooper, J. Propul. Power **9**, 757–763 (1993).
16. E. Ahedo and M. Merino, Phys. Plasmas **18**, 053504 (2011).
17. A. V. Arefiev and B. N. Breizman, Phys. Plasmas **12**, 043504 (2005).
18. K. Takahashi and A. Ando, Phys. Rev. Lett. **118**, 225002 (2017).
19. J. J. Ramos, M. Merino, E. Ahedo, J. Us, and J. Ramos, Phys. Plasmas **25**, 61206 (2018).
20. B. Bhusan Sahu, L. Wen, and J. G. Han, Phys. Rev. Appl. **10**, 054042 (2018).
21. F. Cannat, T. Lafleur, J. Jarrige, P. Chabert, P. Elias, and D. Packan, Phys. Plasmas **22**, 053503 (2015).
22. B. Wachs and B. Jorns, in Joint Propulsion Conference, Cincinnati (2018), p. 4585.
23. J. M. Beall, Y. C. Kim, and E. J. Powers, J. Appl. Phys. **53**, 3933–3940 (1982).
24. T. D. Rempel, C. W. Spragins, S. C. Prager, S. Assadi, D. J. Den Hartog, and S. Hokin, Phys. Rev. Lett. **67**, 1438–1441 (1991).
25. M. Zuin, R. Cavazzana, E. Martines, G. Serianni, V. Antoni, M. Bagatin, M. Andrenucci, F. Paganucci, and P. Rossetti, Phys. Rev. Lett. **92**, 225003 (2004).
26. B. A. Jorns, C. Dodson, D. M. Goebel, and R. Wirz, Phys. Rev. E **96**, 023208 (2017).
27. S. Correyero, Plasma Sources Sci. Technol. **28**, 095004 (2019).
28. R. B. Lobbia and B. E. Beal, J. Propul. Power **33**, 566–581 (2017).
29. J. M. Little and E. Y. Choueiri, Phys. Plasmas **20**, 103501 (2013).
30. R. Geller, *Electron Cyclotron Resonance Ion Sources and ECR Plasmas* (Institute of Physics, United Kingdom, 1996).
31. B. A. Jorns, I. G. Mikellides, and D. M. Goebel, Phys. Rev. E. **90**, 063106 (2014).
32. S. J. Doyle, A. Bennet, D. Tsifakis, J. P. Dedrick, R. W. Boswell, and C. Charles, Front. Phys. **8**, 32 (2020).
33. A. Aanesland, C. Charles, M. A. Lieberman, and R. W. Boswell, Phys. Rev. Lett. **97**, 075003 (2006).
34. N. A. Krall and P. C. Liewer, Phys. Rev. A. **4**, 2094–2103 (1971).
35. T. A. Carter, H. Ji, F. Trintchouk, M. Yamada, and R. M. Kulsrud, Phys. Rev. Lett. **88**, 015001 (2002).
36. T. A. Carter, M. Yamada, H. Ji, R. M. Kulsrud, and F. Trintchouk, Phys. Plasmas **9**, 3272–3288 (2002).
37. C. S. Olsen, M. G. Ballenger, M. D. Carter, F. R. Chang Diaz, M. Giambusso, T. W. Glover, A. V. Ilin, J. P. Squire, B. W. Longmier, E. A. Bering *et al.*, IEEE Trans. Plasma Sci. **43**, 252–268 (2015).
38. M. Giambusso, "Investigation of high frequency instabilities in the plume of the VX-200 magnetic nozzle," Ph.D. thesis (University of Houston, 2018).
39. W. Daughton, G. Lapenta, and P. Ricci, Phys. Rev. Lett. **93**, 105004 (2004).
40. F. Huang, Y. Chen, H.-O. Peng, J.-G. Zheng, G.-F. Shi, and Z.-Q. Hu, Phys. Rev. E. **80**, 056401 (2009).
41. V. Roytershteyn, W. Daughton, H. Karimabadi, and F. S. Mozer, Phys. Rev. Lett. **108**, 185001 (2012).
42. T. K. M. Nakamura, T. Umeda, R. Nakamura, H. S. Fu, and M. Oka, Phys. Rev. Lett. **123**, 235101 (2019).
43. S. D. Bale, F. S. Mozer, and T. Phan, Geophys. Res. Lett. **29**, 33-1–33-4, https://doi.org/10.1029/2002GL016113 (2002).
44. M. Merino and E. Ahedo, Phys. Plasmas **23**, 023506 (2016).
45. S. Migliuolo, J. Geophys. Res. **90**, 377–385, https://doi.org/10.1029/JA090iA01p00377 (1985).
46. A. Hirose and I. Alexeff, Nucl. Fusion **12**, 315–323 (1972).
47. R. C. Davidson and N. T. Gladd, Phys. Fluids **18**, 1327–1335 (1975).
48. M. P. Georgin, B. A. Jorns, and A. D. Gallimore, Phys. Plasmas **26**, 082308 (2019).
49. L. Spitzer and R. Haem, Phys. Rev. **89**, 977–981 (1953).
50. J. P. Boeuf and L. Garrigues, Phys. Plasmas **25**, 061204 (2018).
51. E. Ahedo and M. Merino, Phys. Plasmas **19**, 083501 (2012).
52. B. Wachs and B. Jorns, Plasma Sources Sci. Technol. **29**, 045002 (2020).
53. E. Ahedo and M. Merino, in International Electric Propulsion Conference, Wiesbaden, Germany (IEPC-2011) (2011), No. 2011-050.
54. J. W. S. Cook, S. C. Chapman, R. O. Dendy, and C. S. Brady, Plasma Phys. Controlled Fusion **53**, 065006 (2011).
55. B.-W. Koo, N. Hershkowitz, and M. Sarfaty, J. Appl. Phys. **86**, 1213–1220 (1999).
56. P. C. Stangeby, J. Phys. D **15**, 1007 (1982).
57. W. Varhue, J. Burroughs, and W. Mlynko, J. Appl. Phys. **72**, 3050–3057 (1992).